

Coordinated Motion and Force Control of Multi-Limbed Robotic Systems

Steven Dubowsky¹, Craig Sunada¹ and Constantinos Mavroidis²

¹Department of Mechanical Engineering,
Massachusetts Institute of Technology,
77 Massachusetts Avenue, Cambridge, MA, 02139,
dubowsky@mit.edu

²Department of Mechanical and Aerospace Engineering,
Rutgers University, The State University of New Jersey
98 Brett Road, Piscataway, NJ, 08854
mavro@jove.rutgers.edu

ABSTRACT

This analytic and experimental study proposes a control algorithm for coordinated position and force control for autonomous multi-limbed mobile robotic systems. The technique is called Coordinated Jacobian Transpose Control, or CJTC. Such position/force control algorithms will be required if future robotic systems are to operate effectively in unstructured environments. Generalized Control Variables, GCV's, express in a consistent and coordinated manner the desired behavior of the forces exerted by the multi-limbed robot on the environment and a system's motions. The effectiveness of this algorithm is demonstrated in simulation and laboratory experiments on a climbing system.

1 INTRODUCTION

Advanced autonomous mobile robotic systems could perform important work in field environments such as in the sea, in space, and at nuclear sites (Meieran and Gelhaus 1986, Harmon 1988, Woodbury 1990 and Wilcox et al. 1992). However, these missions present some challenging technical problems. Such systems will need to interact with and manipulate the physical environment, possibly moving heavy obstacles as well as handling fragile objects. Hence, they will need to be able to apply substantial and well controlled forces and torques and also control their motions. Current designs of field robotic systems generally involve a relatively simple vehicle for mobility, such as a submarine or a tracked vehicle, which carries one or two limbs attached to it for manipulation. Clearly significant advantage could be gained in some

cases if a field robotic system had multi-purpose limbs usable for both locomotion and manipulation, see Figure 1.

New control approaches must be developed to simultaneously control the motions of articulated multi-limbed mobile robotic systems and the forces that they exert on their environment or tasks. It would be highly desirable if these motions and forces could be controlled in a coordinated and consistent fashion, one which does not require the continual switching of algorithms as a function of the system's contact configuration with its task and environment.

Here, such an approach is proposed for the control of multi-limbed, multi-degree of freedom robotic systems. It is based on an extension of jacobian transpose control, called Coordinated Jacobian Transpose Control, or CJTC. It uses the notion of Generalized Control Variables, GCV's, to command the system's forces and motions in a consistent and coordinated manner without force feedback. The method is very simple to implement and requires very low computational capabilities. As in classical Jacobian Transpose Control, CJTC is based on the assumption that the system dynamic effects are reduced. This assumption can be verified in multi-limbed robots that have highly geared transmissions. The effectiveness of CJTC is demonstrated in simulation and laboratory experiments on a multi-limbed climbing system, called Limbed Intelligent Basic Robotic Ascender, or LIBRA (Argaez 1993). This approach may contribute to the design of controllers that will enable multi-limbed robotic systems to perform complex tasks in unstructured environments more successfully.

2 BACKGROUND AND LITERATURE

Many control approaches have been used to achieve a stable and accurate position and force control of fixed base serial manipulators. Whitney (1977), in one of the earliest force control approaches described the notion of a generalized damper to control the manipulator forces. Mason (1981) set a theoretical framework for a hybrid control and its relationship to task constraints. Lozano-Perez et. al. (1984) built on this to describe a formal method for planning generalized-damper commands to carry out assembly tasks. Raibert and Craig (1981) proposed a scheme to control manipulator motions to satisfy position and force constraints simultaneously,

and have demonstrated this approach through controlling the end-effector of a two link fixed-based manipulator. Hogan (1985 a, b, c, 1991) introduced impedance control, which controls a relationship between force and displacement, as a unified method for controlling the force and the position of a manipulator's end-effector. Khatib (1987) showed how generalized joint torques are reflected at the end-effector for redundant manipulators, an important understanding for the active force control of redundant manipulators. Seraji (1989) used an augmented Jacobian matrix and manipulator "self motion" functions to resolve redundancy in serial manipulators, with the suggestion it can be extended to multi-arm robots. An overview of robot force control can be found in Whitney (1987) and in Zeng and Hemami (1997.)

A number of researchers have extended these control schemes to the problem of controlling position and force of two fixed-base planar serial manipulators handling a single object. Yoshikawa and Zheng (1993) extended hybrid position/force control to multiple robot manipulators working in a well-known environment. Schneider and Cannon (1992) used Hogan's impedance control approach to arrive at an object impedance controller for cooperative manipulation. Russakow, Khatib and Rock (1995) used an extension of the operational space formulation to control serial-to-parallel chain (branching) manipulators. A number of control algorithms have also been developed for manipulators mounted on moving or vibrating structures such as free-floating spacecrafts (Papadopoulos and Dubowsky 1991a), suspension vehicles (Hootsmans and Dubowsky 1991), long reach manipulators (Mavroidis et al. 1997) and mobile vehicles (Perrier et al. 1996.)

Many multi-limbed robotic systems have been fabricated. The robots Attila, Genghis, Hannibal (Angle 1991) and Boadicea (Binnard 1995) built at the Artificial Intelligence Laboratory at MIT are some examples of small size walking robots. Some climbing robots have been built such as the robots Robug II and III (Luk et al. 1991 and Stone et al. 1995), and Ninja-I (Nagakubo and Hirose 1994). Such climbing robots can be used for wall inspection, fire fighting, underwater cutting or in building construction (Haferkamp et al. 1994, Bach et al. 1995, Nishi 1996).

Most often these systems are controlled with simple joint PID controllers. Advanced controllers such as optimal state feedback and m-synthesis control have been used for the control of walking robots (Channon et al. 1996 and Pannu et al. 1996.) Usually these methods do not control the forces a system exerts on the environment which is very important in many applications such as walking in a rough terrain. Cartesian space controllers, using direct force feedback to control the forces applied to unknown terrain for walking in uncertain or partially known environments, have been proposed in (Gorinevsky and Schneider 1990, Yoneda et al. 1994, Fujimoto and Kawamura 1996, Celaya and Porta 1996.) However, direct force feedback of all the robot-environment forces and moments may not always be possible for a multi-limbed robot. Model based cartesian space controllers, that use the system full dynamic model have occasionally been applied to walking robots (Shih et al. 1993.) However, these methods can be difficult to implement on multi-limbed mobile robots, because full dynamic models of the robot and environment are needed. Additionally, mobile platforms with limited computational capabilities may not be able to implement these computationally expensive controllers. A simple method that tries to control the forces acting on the body of a biped walking robot by virtual model control (Pratt J. 1997) has been proposed.

In summary, to date very little work has been done to control in a coordinated manner the position and forces of mobile multi-limbed systems interacting with its environment through several contact points, without the need of direct force feed-back.

3 ANALYTICAL DEVELOPMENT

A physically diverse set of robotic systems can be represented by a multi-limbed robotic system, including walking and climbing machines, robotic devices with parallel mechanisms, cooperating manipulators and serial manipulators mounted on vehicles.

A representative n-limbed robotic system is shown in Figure 1. This system contains a main body with the i-th limb attached to the body at point B_i , and a base which represents the ground or a stationary task. Contact between the i-th limb and the ground occurs at point C_i .

Some of the limbs position the main body with respect to ground, while the remaining limbs may perform manipulation tasks or be free.

The i -th limb is represented by an m_i joint serial chain where l_i ($l_i \leq m_i$) of the joints are active while $(m_i - l_i)$ joints are passive. Among the $(m_i - l_i)$ passive joints, some are due to the physical contact of the limb with some object such as the ground or a manipulated object and the others are mechanical passive elements such as springs. The total number of active joints for the system is given by $s = \sum_1^n l_i$.

The kinematic variables q_i (i.e. an angle for a revolute joint or a length for a prismatic joint) of a multi-limbed robotic system, of the form described above, form the s by 1 *joint vector* \mathbf{q} where s is the number of active joints. The effort variables of the system's actuators, a torque for a revolute joint or a force for a prismatic joint, are the inputs to the system; they form the s by 1 *input vector* \mathbf{u} .

Any differentiable mathematical function of \mathbf{q} with non-zero first partial derivatives with respect to \mathbf{q} , that describes a physical property of the system is defined to be a ***generalized control variable***. For instance, the Cartesian coordinates x, y, z of a point on the system are functions of \mathbf{q} and are three possible control variables. The set of chosen control variables is called the ***control vector*** \mathbf{u} . The space of control vectors corresponding to all possible configurations of the system is called the ***control space***.

The proposed control algorithm is the Coordinated Jacobian Transpose Control. As in classical Jacobian Transpose Control (Hogan 1985 a, b, c), each element of the control vector \mathbf{u} is forced to move towards its corresponding element of a desired or commanded control vector \mathbf{u}_c by a virtual force \mathbf{F} . For example, \mathbf{F} can be the force of a set of virtual springs and dampers as in a classical impedance control approach. In Figure 2 this concept is shown schematically applied to a multi-limbed robotic system. In this figure the various springs and dampers correspond to a particular set of controlled variables.

The generalized control variables need not be simply the Cartesian coordinates of a free end-effector: they can be Cartesian coordinates of different points and orientations of various

frames on the robot, or more abstract functions of \mathbf{q} such as a system's potential energy. In a more general sense, the control variables can be any differentiable function of the joint vector \mathbf{q} . For example, a control variable could be the maximum height of the multi-limbed robot, so that it can be controlled to crawl through a low tunnel or it can be the system's static stability function to prevent the robot from tipping over.

Hence, the control vector \mathbf{u} can be given in the general form:

$$\mathbf{u}(\mathbf{q}) = [\mathbf{x}(\mathbf{q}), \quad \theta(\mathbf{q}), \quad V(\mathbf{q})]$$

where $\mathbf{x}(\mathbf{q})$ are Cartesian coordinates of specific points of the system, $\theta(\mathbf{q})$ are orientation angles of various frames defined on the system, and $V(\mathbf{q})$ are functions of the configuration of the system, such as potential energy.

In this paper, the control force vector \mathbf{F} , composed of r elements f_i , is defined to be:

$$\mathbf{F} = \mathbf{K}_p [\mathbf{u}_c - \mathbf{u}] + \mathbf{K}_d [\dot{\mathbf{u}}_c - \dot{\mathbf{u}}] \quad (1)$$

where \mathbf{u}_c and $\dot{\mathbf{u}}_c$ are the commanded values of the generalized coordinates. Recall that \mathbf{F} can be any single valued function of \mathbf{u} , \mathbf{u}_c and their time derivatives. The advantage of the force given by Equation (1) is its passive character. As a result, stability issues for such a controller are greatly simplified.

Each one of the forces f_i result in a motion of the system if u_i is free, that is the motion in the corresponding direction to u_i if this direction is not constrained; it results in a force applied to the environment if u_i is constrained. The gain matrices \mathbf{K}_p and \mathbf{K}_d are generally chosen to be diagonal, but can be non-diagonal if coupling between forces f_i is desired. Note that no switching between force and position control of controllers is necessary, giving a unified control structure. The force applied to the environment can be actively controlled by embedding the commanded control variable into the environment.

The joint actuator efforts are obtained by multiplying \mathbf{F} by the system's Jacobian, similar to the classical method:

$$= \mathbf{J}^T(\mathbf{q})\mathbf{F} \quad (2)$$

where the Jacobian is defined as the transformation between joint space velocities and control space velocities:

$$\mathbf{J}(\mathbf{q}) = \begin{matrix} \frac{u_1}{q_1} & \dots & \frac{u_1}{q_s} \\ \vdots & & \vdots \\ \frac{u_r}{q_1} & \dots & \frac{u_r}{q_s} \end{matrix} = \begin{matrix} \frac{x_1}{q_1} & \dots & \frac{x_1}{q_s} \\ \vdots & & \vdots \\ \frac{G_r}{q_1} & \dots & \frac{G_r}{q_s} \end{matrix}$$

The Jacobian is r by s , where r is the number of control variables and s is the total number of active joints. The torque command becomes by adding in a term compensating for gravity:

$$= \mathbf{J}^T(\mathbf{q})\mathbf{F} + \mathbf{G}(\mathbf{q}) \quad (3)$$

Combining (2) and (3), the control algorithm becomes:

$$= \mathbf{J}^T(\mathbf{q})(\mathbf{K}_p[\mathbf{u}_c - \mathbf{u}] + \mathbf{K}_d[\dot{\mathbf{u}}_c - \dot{\mathbf{u}}]) + \mathbf{G}(\mathbf{q}) \quad (4)$$

In Figure 3, the block diagram of the Coordinated Jacobian Transpose Control is shown.

Choosing the control vector \mathbf{u} is not trivial. The designer must choose an admissible set from the infinite number of possible generalized control variables, based on the tasks a specific system must perform, the constraints placed on the system, and desirable performance characteristics. An extended mobility analysis, described in Appendix 1, must be performed to determine the possible control variables (see also Sunada 1994). The i degrees of freedom of a system, under the kinematic constraints imposed by the environment, must be controlled except in special cases (Papadopoulos and Dubowsky 1991b). One actuator can control one degree of freedom. Some interaction forces with the environment can also be controlled if there are more actuators than degrees of freedom ($s > i$); i' degrees of freedom are yielded by relaxing the kinematic constraint with the environment in the desired control direction and performing another mobility analysis. If $s = i'$, then this environmental interaction force can be controlled. Continuing in such a fashion, until $s = i'$ or no more kinematic constraints can be relaxed, leads to the maximum number of control variables to choose. If the number of control variables used is

less than the maximum allowable, i or i' , then some degree of freedom of the system is not being controlled. This is acceptable as long as the uncontrolled degree of freedom does not degrade the performance of the system. Note that the joint space is imposed by the mechanics of the system, while the control space is chosen by the designer.

Consider the system shown in Figure 2 with 18 active joints as an example of the procedure to choose the generalized control variables. Fifteen degrees of freedom are given by a mobility analysis assuming that three legs are in contact with the ground. For manipulation or locomotion tasks, it is important to control the position and the orientation of the main body with respect to the ground. Hence, the $x, y, z, \alpha, \beta, \gamma$ inertial coordinates of the main body (see Figure 2) are 6 control variables. Three degrees of freedom for each free leg are also controlled, and are chosen to be the x, y, z positions of the end-effectors. Then, 15 degrees of freedom controlled and 18 actuators remain, allowing up to 3 constraint forces to be controlled. The $x_3, y_3,$ and y_5 directions might be chosen to be these three. A mobility analysis of the system with these three constraints relaxed results in 18 degrees of freedom controlled by the 18 actuators. The control vector is then:

$$\left[x_b, y_b, z_b, \alpha, \beta, \gamma, x_2, y_2, z_2, x_3, y_3, x_4, y_4, z_4, y_5, x_6, y_6, z_6 \right]^T$$

Coordinated Jacobian Transpose Control for multi-limbed systems has the same advantages that Jacobian Transpose Control offers for serial manipulators. Namely, only the forward kinematics are required, implying a relatively small number of computations. Also, the Jacobian matrix can be rectangular, which is of great importance for redundant systems. Finally, this control scheme provides an intuitively simple interface for controlling end-point positions and forces of a multi-limbed system. By moving the commanded endpoints through space or into an object, the limb moves or pushes accordingly. This allows easy integration with higher level planning algorithms. A complete discussion of these issues is beyond the scope of this paper.

4 AN APPLICATION TO A LABORATORY CLIMBING ROBOT

The CJTC scheme was applied to a planar laboratory climbing system developed at MIT which climbs between two ladders (Argaez 1993). This system is shown schematically in Figure 4. It consists of a main body with three limbs (legs), each with two links, two actuated joints and two passive joints.

The 6 by 1 joint vector, consisting of the angles of the actuated joints, is defined as:

$$\mathbf{q} = [\theta_1, \theta_2, \theta_3, \theta_4, \theta_5, \theta_6]^T$$

The actuated joints are driven by electric motors with a 792:1 gear ratio transmission. This gear ratio was required to produce relatively large torques (20 Nm) using small lightweight motors. The large transmission ratio has several drawbacks, including high friction, poor back-drivability, and significant backlash of two degrees in the output shaft.

The position of the system is defined with respect to the steps of the ladders. The on-board sensors consist of joint angles encoders and a pendulum-based inclinometer that measures the angle of the center body (θ_b). The inclinometer has stiction that limits its sensing to ± 1 degree. A force sensor was mounted on a ladder step to measure the horizontal force applied by foot 2. The sensor was only used for collecting data and did not provide feedback to the control loop. A VME bus computer system running VxWorks is used to control the LIBRA. The control software ran on a 68020 12.5 MHz processor called Blue Slave, and had a cycle rate of 300 Hz. A multi-axis control board mounted on the VME bus called the Programmable Multi Axis Controller (PMAC) (Delta Tau Data Systems 1995) is used to decode and count the encoder signals and as a D/A converter to output the control signals. In Figure 5, a schematic of the electronic configuration of LIBRA is shown.

Application of the extended mobility analysis described in Appendix 1, shows that the system has five degrees of freedom and six actuators. By relaxing the kinematic constraint of foot 2 in the x direction, six degrees of freedom are obtained using the six actuators. The six control variables were chosen with respect to a Cartesian coordinate frame (see Figure 4) as:

$$\mathbf{u} = [x(b), y(b), \theta(b), x(2), x(3), y(3)]^T$$

where $x(b)$, $y(b)$ and $\theta(b)$ are the position and orientation coordinates of the body, $x(2)$ is the coordinate in the x-direction of the tip of the second foot, and $x(3)$ and $y(3)$ are the position coordinates of the tip of the third foot which is the free foot (see Figure 4.)

Since the $x(2)$ variable is constrained by the ladder, the force of the foot in the x-direction is controlled by implanting the commanded control variable into the ladder.

The force equation, as given by Equation (1) is

$$\mathbf{F} = \mathbf{K}_p \begin{bmatrix} x_c(b) - x(b) \\ y_c(b) - y(b) \\ \theta_c(b) - \theta(b) \\ x_c(2) - x(2) \\ x_c(3) - x(3) \\ y_c(3) - y(3) \end{bmatrix} + \mathbf{K}_d \begin{bmatrix} \dot{x}_c(b) - \dot{x}(b) \\ \dot{y}_c(b) - \dot{y}(b) \\ \dot{\theta}_c(b) - \dot{\theta}(b) \\ \dot{x}_c(2) - \dot{x}(2) \\ \dot{x}_c(3) - \dot{x}(3) \\ \dot{y}_c(3) - \dot{y}(3) \end{bmatrix} \quad (5)$$

where the subscript "c" denotes the commanded or desired value of each control variable. The matrices \mathbf{K}_p and \mathbf{K}_d were chosen to be diagonal, with terms of:

$$\mathbf{k}_p = (k_{pb}, k_{pb}, k_{p\theta}, k_{p2}, k_{p3}, k_{p3}) \text{ and } \mathbf{k}_d = (k_{db}, k_{db}, k_{d\theta}, k_{d2}, k_{d3}, k_{d3})$$

corresponding to the spring and damping constants respectively for each control variable.

For the gravity term in Equation (4) the mass of the system was assumed to be considered at a point at the center of the main body. This resulted in good experimental results and was computationally inexpensive. The gravity force due to this lumped mass model is transformed into joint torques using the transpose of the system's Jacobian matrix. The gravity term in (4) then becomes:

$$\mathbf{G}(\mathbf{q}) = \mathbf{J}^T [0, M_g, 0, 0, 0, 0]^T \quad (6)$$

Combining Equations (4), (5), and (6), the input vector becomes:

$$= \begin{bmatrix} 1 \\ 2 \\ 3 \\ 4 \\ 5 \\ 6 \end{bmatrix} = \mathbf{J}^T \mathbf{K}_p \begin{bmatrix} x_c(b) - x(b) \\ y_c(b) - y(b) \\ \theta_c(b) - \theta(b) \\ x_c(2) - x(2) \\ x_c(3) - x(3) \\ y_c(3) - y(3) \end{bmatrix} + \mathbf{K}_d \begin{bmatrix} \dot{x}_c(b) - \dot{x}(b) \\ \dot{y}_c(b) - \dot{y}(b) \\ \dot{\theta}_c(b) - \dot{\theta}(b) \\ \dot{x}_c(2) - \dot{x}(2) \\ \dot{x}_c(3) - \dot{x}(3) \\ \dot{y}_c(3) - \dot{y}(3) \end{bmatrix} + \begin{bmatrix} 0 \\ M_g \\ 0 \\ 0 \\ 0 \\ 0 \end{bmatrix} \quad (7)$$

A dynamic simulation was used to select the control gain matrices \mathbf{K}_p and \mathbf{K}_d . A detailed description of the design specifications and gains selection is given in Appendix 2.

In this section, data are presented for the first stage of a climbing gait and for a full climbing cycle. These data are representative of the performance of the LIBRA under CJTC, and demonstrate the effectiveness of CJTC.

Experimental data from climbing stage one

Figure 6 shows the desired motion for the climbing robot. This is the first stage of a four stage climbing gait. The trajectory consists of the body moving in nearly vertical motion while swinging the third foot over and placing it on a step. Although the body angle $\theta(b)$ is not shown in Figure 6, it is always commanded to be equal to zero. The second foot is pressing against the step with a commanded force of 10 Newtons. This force is specified by moving the commanded control variable $x_c(2)$ into the wall, at distance of $10\text{N} / 900\text{N/m} = 0.011\text{ m}$. Although some physical compliance exists between the foot and the wall, the commanded force remains constant by commanding a constant offset distance from the actual position.

Figures 7 and 8 show the position and orientation coordinates $x(b)$, $y(b)$ and $\theta(b)$ of the experimental trajectory of the main body as a function of time. It can be seen that the main body reaches its steady-state position at approximately 4.5 seconds. During the vertical movement, the x-body position $x(b)$ varies by as much as 5 mm, but remains within 2 mm once the steady-state position is reached. The y-body control variable $y(b)$ followed the desired vertical motion very accurately as shown in Figure 7, and the steady state error is almost 0. The body angle $\theta(b)$ remained within 3×10^{-2} radians, or 1.7 degrees, at all times. The plateaus seen in Figure 8 are caused by stiction in the inclinometer.

The foot force stayed within 4 Newtons of the commanded force of 10 Newtons, even though there is no force feedback. The foot force varies, as with the $x(b)$, during the vertical motion, but steadies once the movement is finished. The force response exceeded the design goals. The force applied by foot 2 in the x direction is shown in Figure 9.

The third foot contacts the ladder at approximately 4 seconds, and the growing apparent position error in $x(3)$ shown in Figure 10 is actually an offset position required to produce the

desired force being applied against the step corresponding to (error/k_{p3}) . The foot is commanded to apply this force on the step to insure a smooth transition to the next phase of the climbing gait. It should be noted that as the foot 3 contact force increases the force at foot 2 is held essentially constant at its desired value by the controller. The $y(3)$ positions, not shown here, are well behaved.

Experimental data from a full climbing cycle

The dotted lines in Figure 11 show the desired trajectories of LIBRA's free foot at each stage of climbing. It is also shown the desired trajectory of LIBRA's body during a full climbing cycle. This is intended to give a qualitative understanding of the gross movement performed, and the detailed data for the individual control variables are given in Figures 12-14. When the commanded control variable for foot 2 or foot 3 is imbedded in the wall, a controlled force is being exerted on the environment.

Figure 12 shows the desired and actual positions of the main body for the climb. The errors are relatively small, and indicate good performance of the system. Figures 13 and 14 show the x and y positions of all the feet during the climb. In Figure 13, the ladder step is located at $x=0.45\text{m}$. Even when the foot is pressing against the ladder, it still appears to move due to the backlash in the actuators and the compliance of the wheels. The commanded positions above 0.45 m indicate that forces are being commanded that are proportional to the error signal. In Figure 14, the steps are located at -0.135m , 0.0m and $+0.135\text{m}$. As can be clearly seen, the tracking for both the x and y of the feet is generally very accurate. Looking at the data for a full climb, it is clear that the controller performed well, tracking the commanded trajectory. Even when joint limits were reached, the controller still continued to function and track the trajectories of control variables that it was physically capable of following. Even though force data was not collected it is assumed that the force was also well controlled.

5 CONCLUSIONS

The Coordinated Jacobian Transpose Control is proposed here as a method for controlling multiple control variables for both position and force of multi-limbed robotic systems in a unified and coordinated manner. One of its advantages is that it is relatively easy to understand and can be interfaced with higher level planners and controllers in a straightforward way using the concept of generalized control variables (GCV's). The GCV's are not restricted to positions of the system. They may be other differentiable functions of the joint variables, giving the system the ability to control important functions of the system in a simple fashion. For example, one could select the potential energy of the system as a control variable to help insure statically stable system postures. Linear analysis, non-linear simulations and experimental studies of a three legged climbing robot suggest that the approach may provide a stable and effective control strategy for mobile multi-limbed systems. Good performance was seen experimentally even though only kinematics and gravity were taken into account. In unstructured environments, the method will also work well, provided that the location of the constraint with respect to the robot can be detected. This can easily be done having simple contact sensors (not force/torque sensors) attached at the tip of the limbs.

6 ACKNOWLEDGMENTS

The support of this work by NASA under Grant NAG-1-801 is acknowledged.

7 REFERENCES

- Angle, C. 1991. *Design of an Artificial Creature*. M.S. Thesis, Department of Electrical Engineering, MIT, Cambridge, MA.
- Argaez, D.A. 1993. *An Analytical and Experimental Study of the Simultaneous Control of Motion and Force of a Climbing Robot*. M.S. Thesis, Department of Mechanical Engineering, MIT, Cambridge, MA.
- Bach, F., Rachkov, M., Seevers, J. and Hahn, M. 1995. High Tractive Power Wall-Climbing Robot. *Automation in Construction*, 4(3):213-224.
- Binnard M. 1995. *Design of a Small Pneumatic Walking Robot*. M.S. Thesis, Department of Mechanical Engineering, MIT, Cambridge, MA.
- Celaya, E. and Porta, J. 1996. Control of a Six-Legged Robot Walking on Abrupt Terrain. In *Proceedings of the IEEE International Conference on Robotics and Automation*, Minneapolis, MN, pp. 2731-2736.

- Channon, P.H., Hopkins, S.H., Pham, D.T. 1996. Optimal Control of an n-legged Robot. *Journal of Systems & Control Engineering*, 210(1): 51-63.
- Delta Tau Data Systems, Inc., 1995. *PMAC Executive v3.1*.
- Fujimoto, Y. and Kawamura, A. 1996. Proposal of Biped Walking Control Based on Robust Hybrid Position/Force Control. In *Proceedings of the IEEE International Conference on Robotics and Automation*, Minneapolis, MN, pp. 2724-2730.
- Gorinevsky, D. and Schneider, A. 1990. Force Control in Locomotion of Legged Vehicles over Rigid and Soft Surfaces. *The International Journal of Robotics Research*, 9(2): 4-23.
- Haferkamp, H., Bach, F., Ogawa, Y. and Rachkov, V. 1994. Climbing Robot For Underwater Cutting. In *Proceedings of the IEEE Oceans Conference*, Brest, France, 1:602-607.
- Harmon, S.Y. 1988. A Report on the NATO Workshop on Mobile Robot Implementation. In *Proceedings of the 1988 IEEE International Conference on Robotics and Automation*, Philadelphia, PA, pp. 604-610.
- Hogan, N. 1985a. Impedance Control: An Approach to Manipulation: Part I--Theory. *Transactions of the ASME, Journal of Dynamic Systems, Measurement and Control*, 107:1-7.
- Hogan, N. 1985b. Impedance Control: An Approach to Manipulation: Part II--Implementation. *Transactions of the ASME, Journal of Dynamic Systems, Measurement and Control* 107: 8-16.
- Hogan, N. 1985c. Impedance Control: An Approach to Manipulation: Part III--Applications. *Transactions of the ASME, Journal of Dynamic Systems, Measurement and Control*, 107: 17-24.
- Hogan, N. 1991. Impedance Control of Robots with Harmonic Drive Systems. In *Proceedings of the 1991 American Control Conference*, Boston, MA.
- Hootsmans N. and Dubowsky S. 1991. Large Motion Control of Mobile Manipulators Including Vehicle Suspension Characteristics. In *Proceedings of the 1991 IEEE International Conference on Robotics and Automation*, Sacramento, CA, pp. 2336-2341.
- Khatib, O. 1987. A Unified Approach for Motion and Force Control of Robot Manipulators: The Operational Space Formulation. *IEEE Journal of Robotics and Automation*, RA-3(1):43-53.
- Lozano-Perez, T., Mason, M.T. and Taylor, R. H. 1984. Automatic Synthesis of Fine-Motion Strategies. *The International Journal of Robotics Research*, 3(1): 3-24.
- Luk, B. L., Collie, A.A. and Billingsley, J. 1991. Robug II: An Intelligent Wall Climbing Robot. In *Proceedings of the IEEE International Conference on Robotics and Automation*, Sacramento, CA, pp. 2342-2347.
- Mason, M. T. 1981. Compliance and Force Control for Computer Controlled Manipulators. *IEEE Transactions on Systems Man and Cybernetics*, SMC-11:418-432.
- Mavroidis, C., Dubowsky, S. and Thomas, K. 1997. Optimal Sensor Location in Motion Control of Flexibly Supported Long Reach Manipulators. *Transactions of the ASME, Journal of Dynamic Systems, Measurement and Control*, 119(4):718:726.
- Meieran, H.B. and Gelhaus, F.E. 1986. Mobile Robots Designed for Hazardous Environments. *Robots and Engineering* 8: 10-16.
- Nagakubo, A. and Hirose, S. 1994. Walking and Running of the Quadruped Wall-Climbing Robot. In *Proceedings of the IEEE International Conference on Robotics and Automation*, San Diego, CA, pp. 1005-1012.
- Nishi, A. 1996. Development of Wall-Climbing Robots. *Computer and Electrical Engineering*, 22(2):123-149.
- Pannu, S., Kazerooni, H., Becker, G., and Packard, A. 1996. m-Synthesis Control for a Walking Robot. *IEEE Control Systems Magazine*, 16(1):20-25.

- Papadopoulos, E. and Dubowsky, S. 1991a. On the Nature of Control Algorithms for Free-Floating Space Manipulators. *IEEE Transactions on Robotics and Automation*, 7:750-758.
- Papadopoulos, E. and Dubowsky, S. 1991b. Failure Recovery Control For Space Robotic Systems. In *Proceedings of the 1991 American Control Conference*, Boston, MA, pp.1485-1490.
- Perrier, C., Cellier, L., Dauchez, P., Fraisse, P., Degoulange, E. and Pierrot, F., 1996. Position/Force Control of a Manipulator Mounted on a Vehicle. *Journal of Robotic Systems*, 13(11):687-698.
- Pratt, J. 1997. Virtual Model Control of a Biped Walking Robot. In *Proceedings of IEEE International Conference on Robotics and Automation*, Albuquerque, NM, pp. 193-198.
- Raibert, M. and Craig, J. 1981. Hybrid Position/Force Control of Manipulators. *Transactions of the ASME, Journal of Dynamic Systems Measurement and Control*, 102:126-133.
- Russakow, J., Khatib, O. and Rock, S. 1995. Extended Operational Space Formulation for Serial-to-Parallel Chain (Branching) Manipulators. In *Proceedings of the IEEE International Conference on Robotics and Automation*, Nagoya, Japan.
- Sandor, G. and Erdman, A., 1984. *Advanced Mechanism Design: Analysis and Synthesis, Volume 2*. Prentice-Hall, Inc., New Jersey.
- Schneider, S.A. and Cannon, R. H. Jr. 1992. Object Manipulation Control for Cooperative Manipulation: Theory and Experimental Results. *IEEE Transactions on Robotics and Automation*, 8(3):383-394.
- Seraji, H. 1989. Configuration Control of Redundant Manipulators : Theory and Implementation. *IEEE Transactions on Robotics and Automation*, 5(4): 472-490.
- Shih, C., Gruver, A., and Lee, T. 1993. Inverse Kinematics and Inverse Dynamics for Control of a Biped Walking Machine. *Journal of Robotics Systems*, 10(5): 531-555.
- Stone, T., Cooke, D. and Luk, B. 1995. Robug III - The Design of an Eight Legged Teleoperated Walking and Climbing Robot for Disordered Hazardous Environments. *Mechanical Incorporated Engineer*, 7(2):37-41.
- Sunada, C. 1994. *Coordinated Jacobian Transpose Control and Its Application to a Climbing Machine*. M.S. Thesis, Department of Mechanical Engineering, MIT, Cambridge, MA.
- Whitney, D. E. 1977. Force Feedback and Control of Manipulator Fine Motions. *Transactions of the ASME, Journal of Dynamic Systems, Measurement and Control* : 91-97.
- Whitney, D. E. 1987. Historical Perspective and State of the Art in Robot Force Control. *The International Journal of Robotics Research*, 6(1):3-14.
- Wilcox, B. et al., 1992. Robotic Vehicles for Planetary Exploration. In *Proceedings of the IEEE International Conference on Robotics and Automation*, Nice, France, 1:175-180.
- Woodbury, R. 1990. Exploring the Ocean's Frontiers Robots and Miniature Submarines Take Oil Drillers to New Depths. *Time*, 17.
- Yoneda, K., Iiyama, H., Hirose., Shigeo S. 1994. Sky Hook Suspension Control of a Quadruped Walking Vehicle. In *Proceedings of the IEEE International Conference on Robotics and Automation*, San Diego, CA, pp. 999-1004.
- Yoshikawa, T. and Zheng, X. 1993. Coordinated Dynamic Hybrid Position/Force Control for Multiple Robot Manipulators Handling One Constrained Object. *The International Journal of Robotics Research*, 12(3):219-230.
- Zeng, G. and Hemami, A. 1997. Overview of Robot Force Control. *Robotica*, 15(5):473-482.

APPENDIX 1: EXTENDED MOBILITY ANALYSIS

The Extended Mobility Analysis, which is based on the classical Gruebler's mechanism mobility analysis (Sandor and Erdman 1984), addresses which sets of control variables can be controlled for a system subject to a given set of environmental constraints. It insures that the control variables chosen are independent, and that the system does not become overconstrained. The basic procedure is to repeatedly perform Gruebler's mobility analysis, adding constraints for the control variables chosen and relaxing environmental constraints to test if an interaction force or moment can be controlled. A flow graph of the Extended Mobility Analysis is given in Figures 15 (a) and (b) where the nomenclature used is: (a) is the number of degrees of freedom (DOF) of the system under the full environmental constraints, (b) is the number of uncontrolled DOF, (r) is the number of control variables selected and (s) is the number of active joints

The first stage of the Extended Mobility Analysis, shown in Figure 15a, deals with choosing control variables to control the available degrees of freedom under the full environmental constraints. Performing a mobility analysis on a multilimbed mobile robot under the full constraints of the environment will yield (a) degrees of freedom ($b=a$). It is assumed all of these degrees of freedom must be controlled for acceptable system performance. If there are less active joints than degrees of freedom ($s < a$), then the system is under actuated and cannot be controlled using this control scheme. To test if a control variable is admissible, a constraint must be placed on it and another mobility analysis run. If the mobility analysis yields the loss of one degree of freedom ($b=b-1$), then the control variable does not overconstrain the system and is admissible. If the mobility analysis does not yield the loss of one degree of freedom ($b=b$), then the control variable cannot be controlled because it is already constrained by the given environmental constraints or the constraints from the previous control variables chosen. If it is highly desirable to control that control variable, then it is still possible to do so either by choosing it later in the analysis as a controlled environmental interaction force, if an environmental constraint is constraining it, or by eliminating one or more previously selected control variables, if the control variable constraints are constraining it. If the control variable is inadmissible and it is not highly desirable to control it, then the constraint is removed and

another control variable tested. After (a) admissible control variables are chosen and constrained, then the system shouldn't have any degrees of freedom ($b=0$). If it does, then the set of a control variables chosen are not independent of each other and cannot be controlled simultaneously. If the number of active joints is greater than the number of degrees of freedom ($s>a$), then it is possible to control a number ($s-a$) of interaction forces with the environment, internal forces, or other control variables. The second stage of the Extended Mobility Analysis must then be performed.

The second stage of the Extended Mobility Analysis, shown in Figure 15b, deals with controlling environmental interaction forces and internal forces. At the start of the second stage, all degrees of freedom of the system are controlled, and $b=0$. To test if a desired interaction or internal force or moment is controllable, a control variable is chosen as the desired interaction force with the environment or internal force, and the environmental position constraint or internal displacement constraint on that control variable is relaxed. With all the other control variables constrained, the system should then have one additional degree of freedom ($b=b+1$). If so, then that force or moment is controllable. To mark that the force or moment is controlled, replace the corresponding constraint with a spring. Note that a spring does not act as a link or constraint for purposes of a mobility analysis and it is merely there to indicate visually that the corresponding interaction force is being controlled. If the system does not have an additional degree of freedom ($b=b$), then that interaction or internal force is not controllable, perhaps due to the other control variables chosen or because the mechanism cannot apply forces in that direction. In this case, restore the original constraint. If there are still more actuators than control variables chosen ($s>r$), then additional control variables can be controlled, if desired.

APPENDIX 2: CONTROL GAIN SELECTION FOR LIBRA

An analysis of a dynamic model of the LIBRA system was used to select the control gain matrices \mathbf{K}_p and \mathbf{K}_d . Only the top chain of the LIBRA was modeled, as it is assumed that the free foot can be analyzed separately. To simplify the model of the LIBRA, point masses m_i are assumed to be located at the positions shown in Figure 16, where: m_1 is the mass of limb link, m_2 is the motor mass, m_3 is the mass of the body, m_{10} is the mass of limb three and K_e is the environmental stiffness

The limb link masses, which are identical for all links, are assumed to be lumped halfway along the links. The motor masses are placed at the joints. The body mass is located at the geometric center of the body. As an approximation, the mass of limb three is assumed to be at the first joint of the third limb. The actuators are also modeled as frictionless torque supplies, ignoring the internal friction and actuator dynamics. While the actuator dynamics are sufficiently fast that they shouldn't affect the dynamics of the overall system, the friction in the actuators will add a significant amount of damping. The dynamic equations are derived using Lagrange's equation:

$$\frac{d}{dt} \frac{T}{\dot{\mathbf{q}}} - \frac{T}{\mathbf{q}} - \frac{V}{\mathbf{q}} - \mathbf{q} = 0 \quad (8)$$

where T is the kinetic energy of the system and V is the potential energy of the system

To further simplify the equations, it is assumed that the gravity compensation term of the controller is exact. The equations are linearized about $\dot{\mathbf{q}} = 0$. In state space form, using the control vector as the state space, these equations can be represented as:

$$\begin{aligned} \begin{bmatrix} \ddot{\mathbf{u}} \\ \dot{\mathbf{u}} \end{bmatrix} &= \begin{bmatrix} \mathbf{J}(\mathbf{q}) \mathbf{H}^{-1}(\mathbf{q}) \mathbf{J}^T(\mathbf{q}) \mathbf{K}_d & \mathbf{J}(\mathbf{q}) \mathbf{H}^{-1}(\mathbf{q}) \mathbf{J}^T(\mathbf{q}) \mathbf{K}_p \\ \mathbf{I} & \mathbf{0} \end{bmatrix} \begin{bmatrix} \dot{\mathbf{u}} \\ \mathbf{u} \end{bmatrix} + \\ & \begin{bmatrix} \mathbf{J}(\mathbf{q}) \mathbf{H}^{-1}(\mathbf{q}) \mathbf{J}^T(\mathbf{q}) \mathbf{K}_d & \mathbf{J}(\mathbf{q}) \mathbf{H}^{-1}(\mathbf{q}) \mathbf{J}^T(\mathbf{q}) \mathbf{K}_p \end{bmatrix} \begin{bmatrix} \dot{\mathbf{u}}_c \\ \mathbf{u}_c \end{bmatrix} \quad (9) \\ [\mathbf{y}] &= \begin{bmatrix} \mathbf{0} & \mathbf{I} \end{bmatrix} \begin{bmatrix} \dot{\mathbf{u}} \\ \mathbf{u} \end{bmatrix} \end{aligned}$$

where \mathbf{H} is the configuration dependent inertia matrix and vector \mathbf{u} is defined in Section 4. Since the terms of the matrices are not constant, but are instead very configuration dependent, the system response changes as a function of the configuration.

Equation (9) is linearized around 18 representative configurations of the system. These points were chosen to reflect the range of motion found in the climbing maneuver. The x_{body} position was chosen to be at one half the wall separation of 0.18 m. The q_{body} is chosen to be zero, which is the commanded position during the entire climbing gait. The x_2 position of foot 2 is chosen to be at the wall. The only control variable in the top kinematic chain that really varies during the climbing gait is the y_{body} , which was chosen to vary from -0.22 m through 0.05 m. This represents the fullest possible vertical movement of the LIBRA in the current climbing setup. Classical root locus methods and bode plots were used to study the stability of the system. The system gains were chosen to meet the design specification of a bandwidth of 6 Hz and steady state positioning errors of the center body of less than 2 mm under a 10 N disturbance. The gains suggested through this analysis were: $k_p = [1000, 1000, 22, 500]$ and $k_d = [160, 160, 4, 120]$. After experimental tests, the gains were tuned to: $k_p = [1000, 500, 8, 100]$ and $k_d = [200, 100, 2, 20]$

The dominant poles for these gains, sampled at different configurations, are given in Figure 17. While it might appear in these diagrams that the system is under damped and the bandwidth is larger than desired, it is important to note that the analysis did not include the damping effects of the friction in the motor gearheads.

The last limb, limb three, was chosen separately to have gains of $k_p = [100, 100]$ and $k_d = [10, 10]$. This selection was strictly based on experimental trial and error. It was found that the gains for the third foot have little effect on the performance of the upper kinematic chain. Also, the third foot performance is not sensitive to the gains chosen, and a wide range of gains could be chosen based on the desired performance of the third foot. Gains of up to $k_p = [1000, 1000]$ and $k_d = [150, 150]$ were used for closer trajectory tracking.

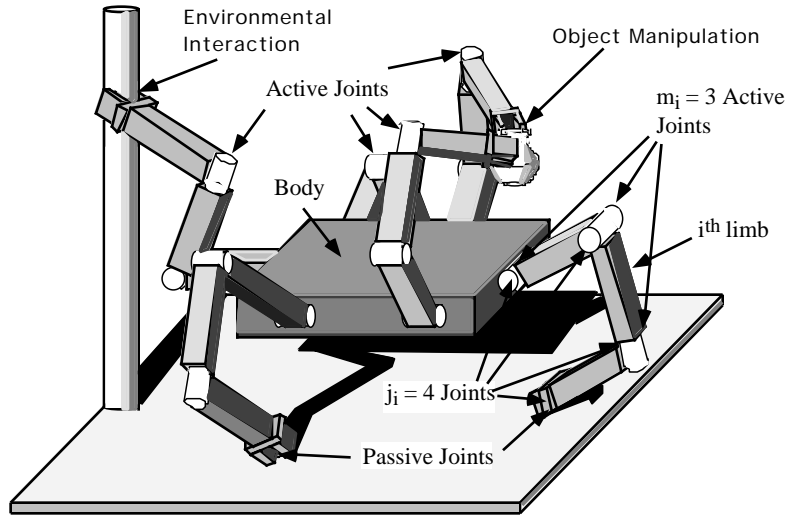


Figure 1: A Schematic of a Multi-Limbed Robot

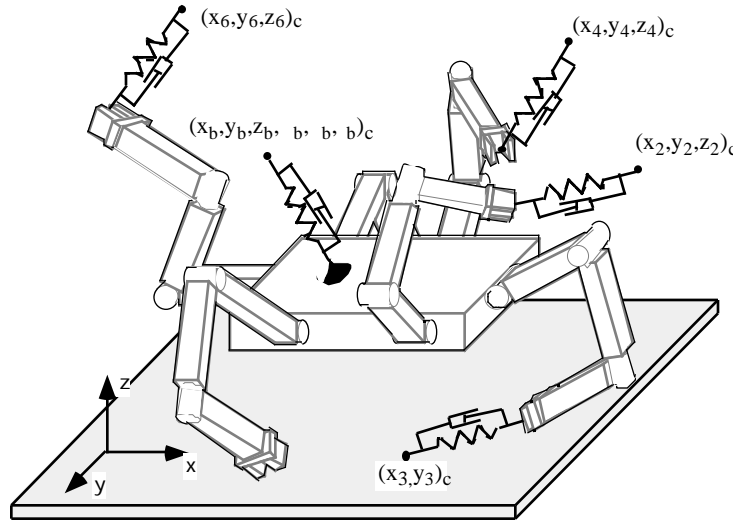


Figure 2: Robotic System With GCVs Attached

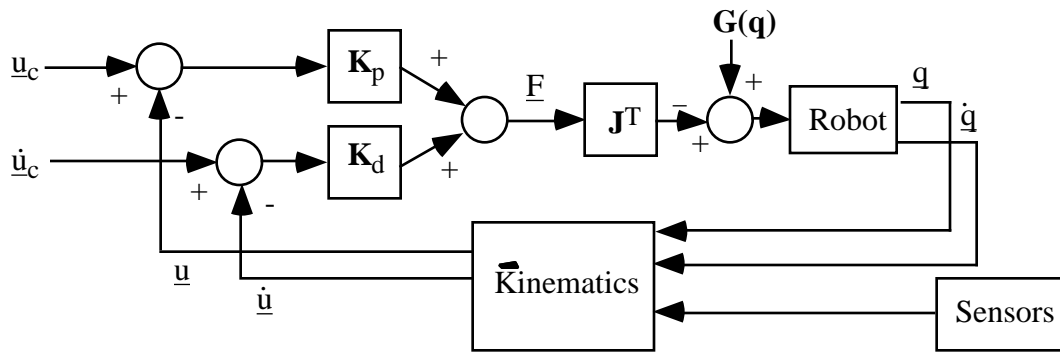


Figure 3: The Coordinated Jacobian Transpose Control Block Diagram

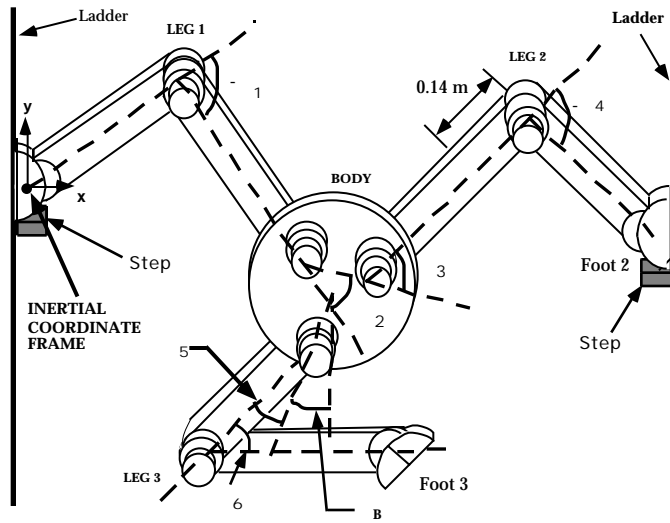


Figure 4: A Schematic of the Climbing System

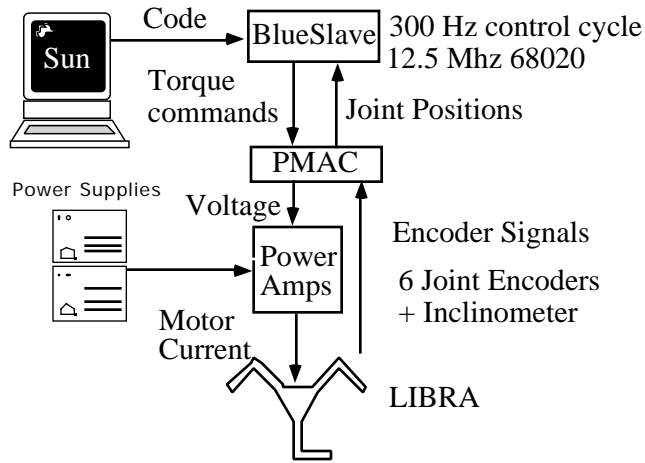


Figure 5: LIBRA's Electronic Architecture

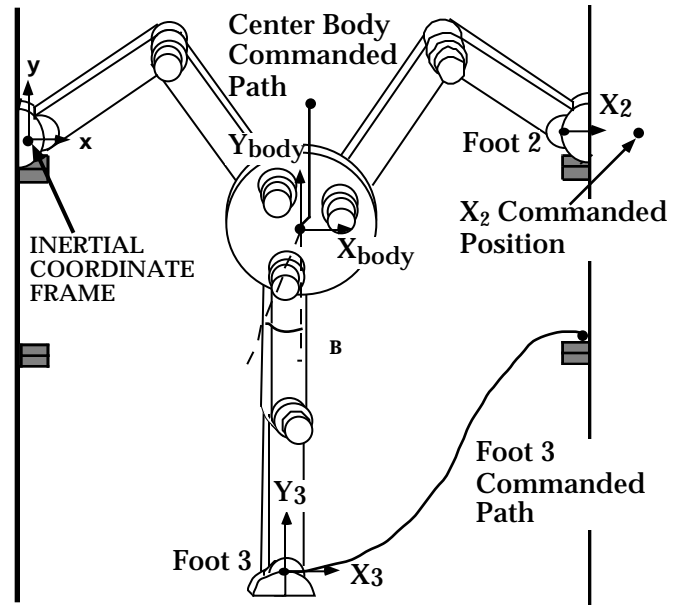


Figure 6: Desired Motion for the Climbing Robot

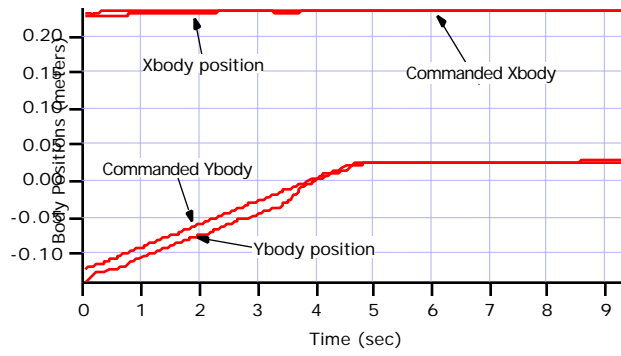


Figure 7: The Body Coordinates $x(b)$ and $y(b)$ for a Pushup Maneuver

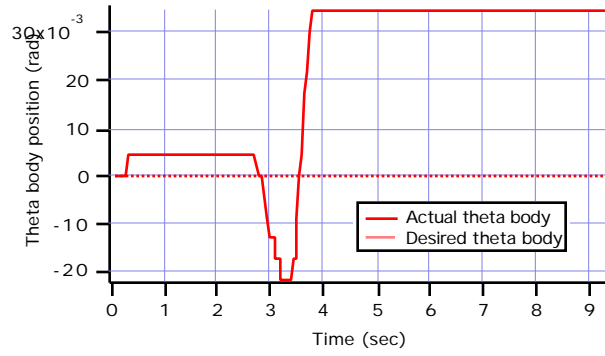


Figure 8: The Body Angle (b) for a Pushup Maneuver

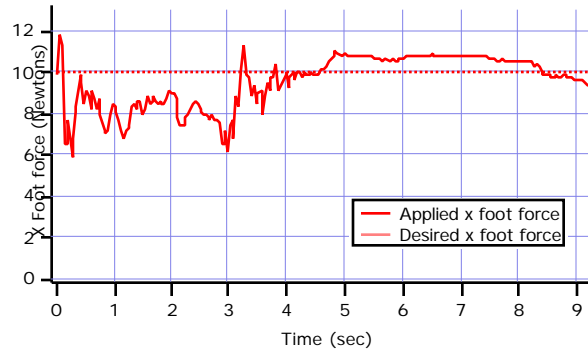


Figure 9: Force of Foot 2 in the x-direction for a Pushup Maneuver

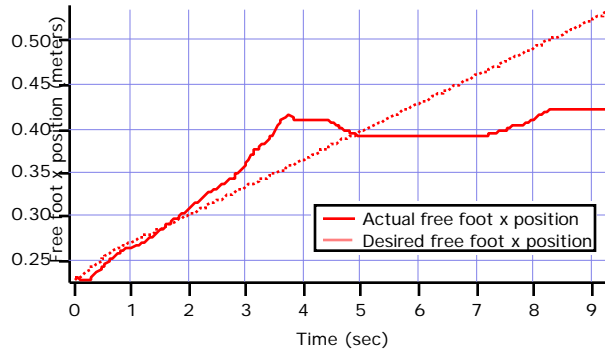


Figure 10 : The Coordinate $x(3)$ of Foot 3 for a Pushup Maneuver

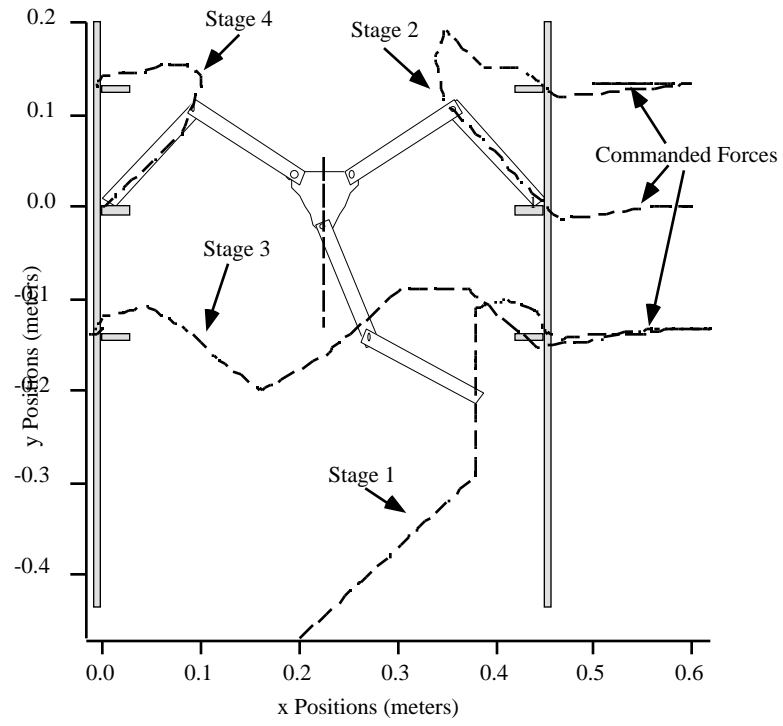


Figure 11: LIBRA's Commanded Trajectory Climbing a Ladder

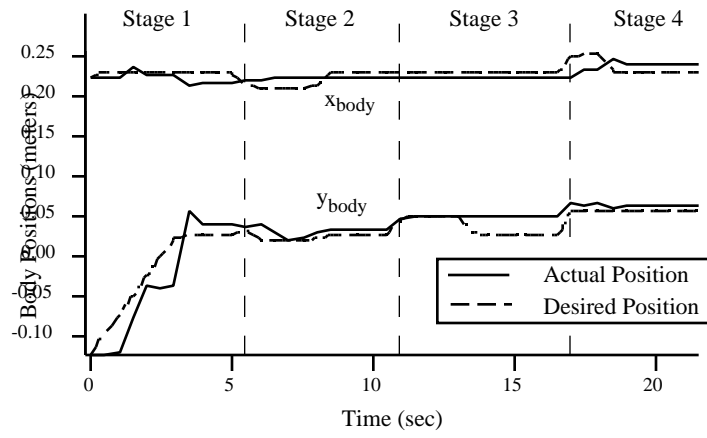


Figure 12: Body Movements for One Gait Cycle

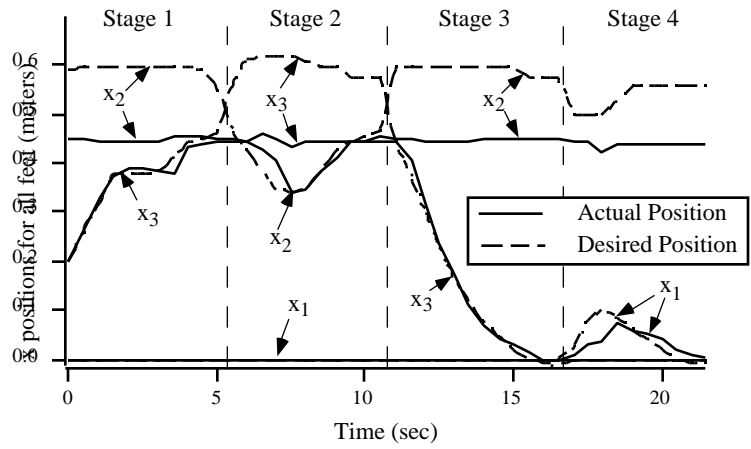


Figure 13: x Positions for All the Feet for One Gait Cycle

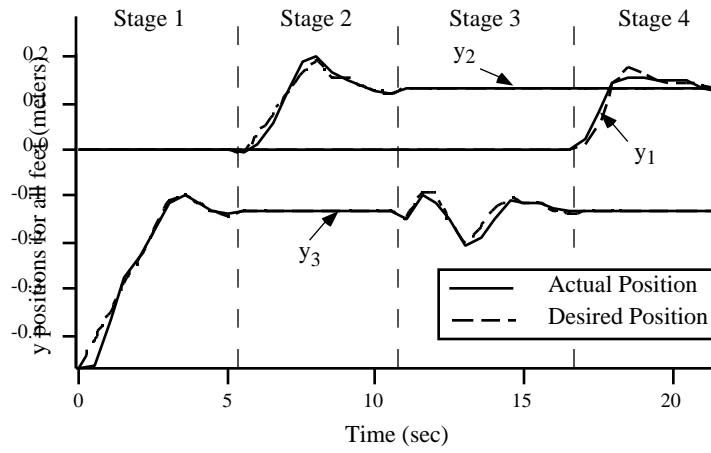
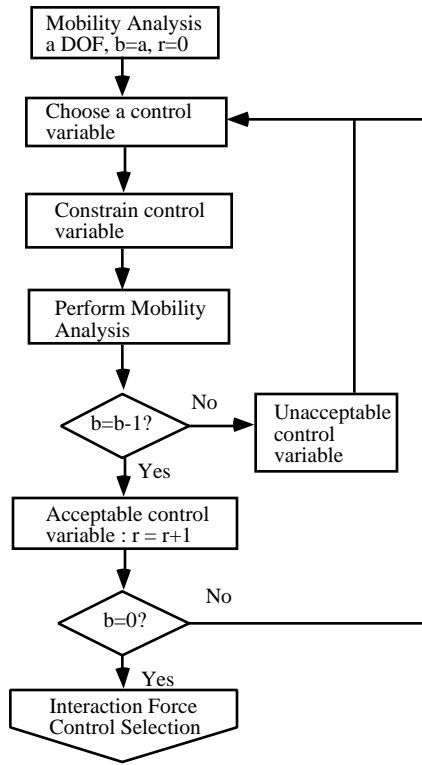
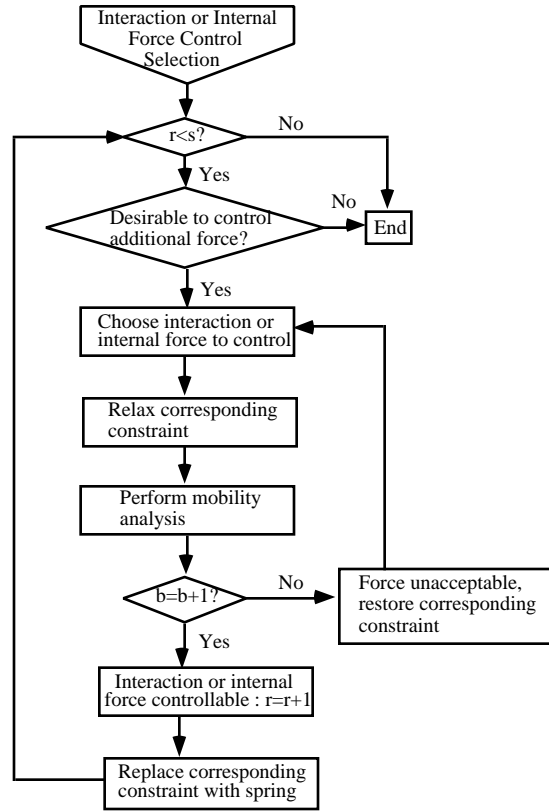


Figure 14: y Positions for All the Feet for One Gait Cycle



(a) Stage One



(b) Stage Two

Figure 15: The Extended Mobility Analysis

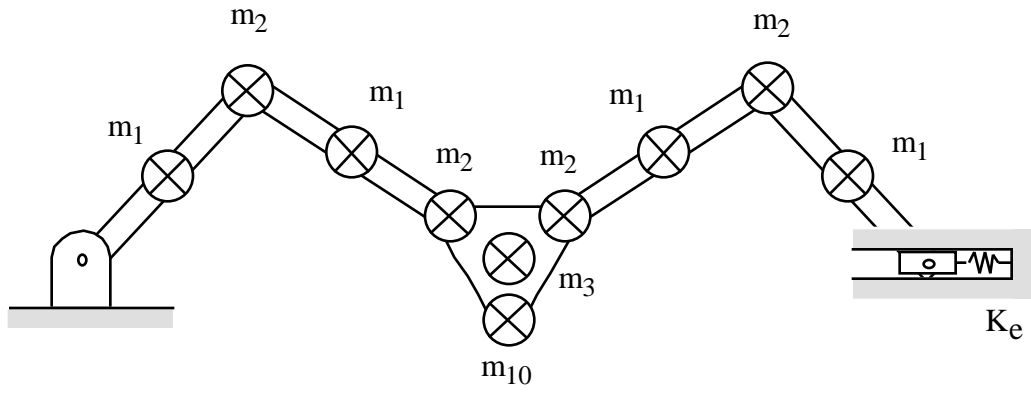


Figure 16: Model of the LIBRA Top Kinematic Chain

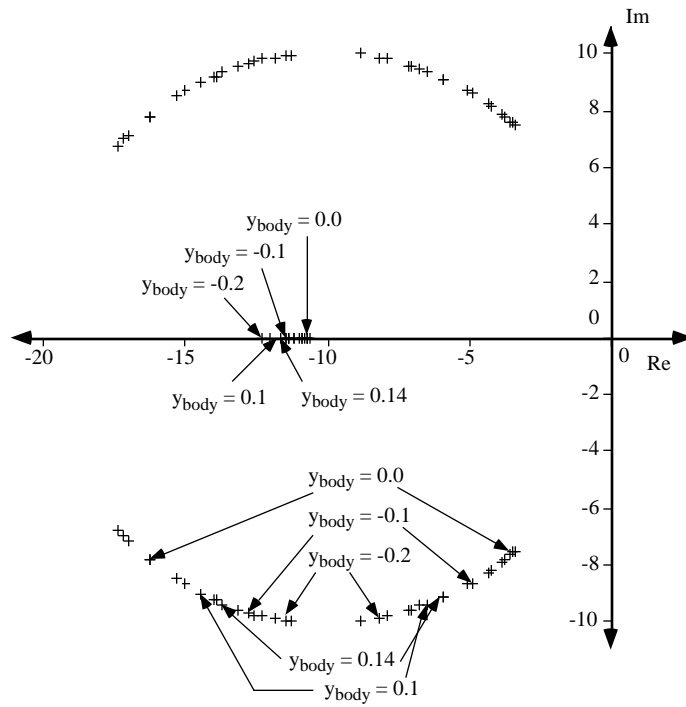


Figure 17: Dominant Poles of the LIBRA for y_{body} from -0.20m \rightarrow 0.14 m